

Focus on Low-Resolution Information: Multi-Granular Information-Lossless Model for Low-Resolution Human Pose Estimation

Zejun Gu, Zhong-Qiu Zhao, Hao Shen, Zhao Zhang

ABSTRACT

In real-world applications of human pose estimation, low-resolution input images are frequently encountered when the performance of the image acquisition equipment is limited or the shooting distance is too far. However, existing state-of-the-art models for human pose estimation perform poorly on low-resolution images. One key reason is the presence of downsampling layers in these models, *e.g.*, strided convolutions and pooling layers. It further reduces the already insufficient image information. Another key reason is that the body skeleton and human kinematic information are not fully utilized. In this work, we propose a Multi-Granular Information-Lossless (MGIL) model to replace the downsampling layers to address the above issues. Specifically, MGIL employs a Fine-grained Lossless Information Extraction (FLIE) module, which can prevent the loss of local information. Furthermore, we design a Coarse-grained Information Interaction (CII) module to adequately leverage human body structural information. To efficiently fuse cross-granular information and thoroughly exploit the relationships among keypoints, we further introduce a Multi-Granular Adaptive Fusion (MGAF) mechanism. The mechanism assigns weights to features of different granularities based on the content of the image. The model is effective, flexible, and universal. We show its potential in various vision tasks with comprehensive experiments. It outperforms the SOTA methods by 7.7 **mAP** on COCO and performs well with different input resolutions, different backbones, and different vision tasks. The code is provided in supplementary material.

CCS CONCEPTS

• **Computing methodologies** → **Computer vision problems; Interest point and salient region detections.**

KEYWORDS

Low-resolution images, human pose estimation, multi-granular Information, adaptive fusion.

1 INTRODUCTION

Human pose estimation aims to localize all human keypoints in a single RGB image. It is the foundation of high-level vision tasks

Permission to make digital or hard copies of all or part of this work for personal or classroom use is granted without fee provided that copies are not made or distributed for profit or commercial advantage and that copies bear this notice and the full citation on the first page. Copyrights for components of this work owned by others than the author(s) must be honored. Abstracting with credit is permitted. To copy otherwise, or republish, to post on servers or to redistribute to lists, requires prior specific permission and/or a fee. Request permissions from permissions@acm.org.

ACM MM, 2024, Melbourne, Australia

© 2024 Copyright held by the owner/author(s). Publication rights licensed to ACM.

ACM ISBN 978-x-xxxx-xxxx-x/YY/MM

<https://doi.org/10.1145/nnnnnnn.nnnnnnn>



Figure 1: Visualization of our proposed MGIL model with low-resolution inputs on the COCO val dataset.

such as action recognition [58], virtual reality [39], and human-computer interaction [34]. In recent years, deep learning has greatly improved the performance of human pose estimation.

Recent works [12, 20, 28, 32, 41, 44, 45, 48, 49, 68, 69, 71–76, 79, 80, 82] on human pose estimation mainly focus on high-resolution images (greater than or equal to 256×192). However, in real-world application scenarios, it is common to encounter low-resolution input images. For example, due to the large size of high-resolution images, saving or processing them on mobile devices is often challenging. Therefore, low-resolution images have to be used to replace them. Additionally, the limited performance of image acquisition devices or excessive shooting distances may result in low-resolution input images. However, the performance of existing SOTA models for high-resolution human pose estimation significantly degrades when applied to low-resolution images. Therefore, it is necessary to explore approaches to improve the accuracy of low-resolution human pose estimation.

Current human pose estimation models usually have downsampling layers (strided convolutional layers or pooling layers), such as CPM [65], Hourglass [36], and HRNet [50]. These downsampling layers can help models save computational costs and remove redundant information. However, when they are applied to low-resolution images, they will further reduce the already insufficient

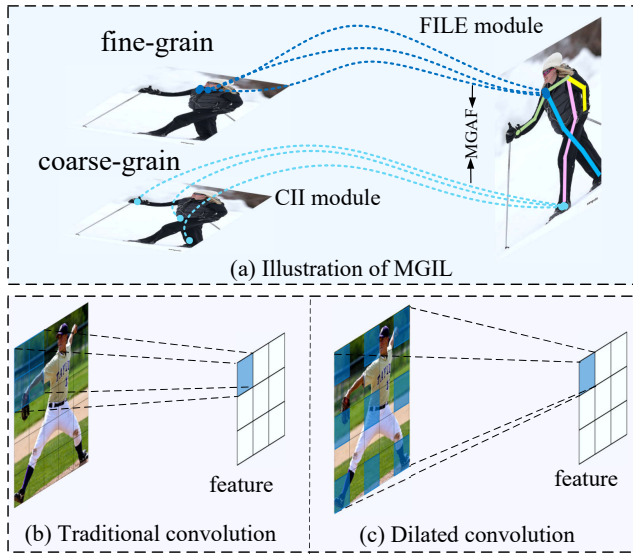


Figure 2: The illustration of the Multi-Granular Information-Lossless (MGIL) Model. The comparison of traditional convolution (b) and dilated convolution (c).

fine-grained information, which hinders the proper learning of features. In addition, traditional convolutions in their models only focus on local information, neglecting the global information that includes keypoints relationships, as shown in Fig. 2 (b). The relational information between keypoints can be leveraged to predict the positions of keypoints based on the human body skeleton structure and human kinematics principles, which is particularly beneficial in conditions of occlusion or blurriness (*e.g.*, low resolution).

To address the above problems, we propose a Multi-Granular Information-Lossless (MGIL) model to replace downsampling layers. In the MGIL model, we introduce a Fine-grained Lossless Information Extraction (FLIE) module to tackle the problem of information loss caused by downsampling. This module first supplements the information lost due to reduced spatial size onto the channels, achieving a lossless transformation of information, and then ensures the information is fully learned through a Lossless Information Extraction (LIE) block. Furthermore, we introduce a Coarse-grained Information Interaction (CII) module to capture information from different receptive fields. The information contains the connectivity and symmetry relationships of the human skeleton which is crucial for keypoint prediction. Finally, we propose a Multi-Granular Adaptive Fusion (MGAF) mechanism to fuse features of different granularities. It can adaptively allocate weights to each feature based on the importance of information at different granularities.

We propose a simple yet sufficiently effective model (MGIL). This model has the following significance: 1) This module ensures that the size of the input and output features remain completely consistent with downsampling layers, thus it can easily replace downsampling layers without any difficulty. 2) This module is versatile, as it can be applied to different convolutional networks, enhancing the performance of various computer vision tasks.

SPD-Conv [51] is a block that replaces downsampling layers to improve performance on low-resolution visual tasks. However, it suffers from the following problems: 1) It only utilizes a non-strided convolution, which results in insufficient learning of feature information. 2) It fails to make full use of the spatial correlation information between distant keypoints. Our proposed MGIL model solves the above problems.

Therefore, our contributions can be summarized as:

- We propose a Multi-Granular Information-Lossless (MGIL) model to replace the downsampling layers to enhance the accuracy of low-resolution human pose estimation.
- This model is universal. It can be transferred to various input resolutions, diverse backbones, and different low-resolution visual tasks (*e.g.*, classification and object detection).
- To our best knowledge, we are the first to propose a universal model at the block level to address low-resolution challenges and apply it to human pose estimation.
- We show the effectiveness of the MGIL model through extensive experiments. Considerable improvements have been observed in all of these comparisons.

2 RELATED WORK

2.1 Human Pose Estimation

In recent years, a substantial amount of work aims to improve the performance of human pose estimation by studying keypoint representation methods, which can be divided into three main directions: heatmap-based methods [2, 4, 5, 9, 29, 54, 62, 66, 77], regression-based methods [3, 6, 53, 55, 56, 81], and other new keypoint representation methods [12, 30]. Heatmap-based methods utilize spatial information around the GT keypoints to create more comprehensive label information. Among the recent heatmap-based studies, some studies [7, 36, 50, 65] aim to enhance the model’s ability to extract feature information by improving the backbone. Sun *et al.* [50] adopt a deep high-resolution keypoint representation method, which has become the best-performing backbone in human pose estimation. Huang *et al.* [15] propose to reduce quantization error to improve prediction accuracy. Some other works [31, 69] utilize transformers to enhance model performance. However, heatmap-based methods have the disadvantage of being inefficient. Regression-based methods are efficient in keypoint prediction by directly regressing the coordinates. Some improved works [11, 64] propose to focus on local features around the joints. Residual log-likelihood [27] estimation introduces a new regression paradigm to capture potential output distributions. They all allow regression-based methods to maintain high efficiency. Nevertheless, regression-based methods have the disadvantage of not being accurate enough. The work [75] combines the advantages of heatmap-based and regression-based methods by means of knowledge distillation. Recently, several studies focus on new keypoint representations for human pose estimation. The works [12, 30] innovatively propose new label representation methods to optimize model learning.

Other studies focus more on practical application issues in human pose estimation. Lee *et al.* [25] introduce ExLPose to address the issue of current models failing to work properly under low-light conditions. Ju *et al.* [19] propose a dataset for human pose estimation in artwork to apply the human pose estimation model

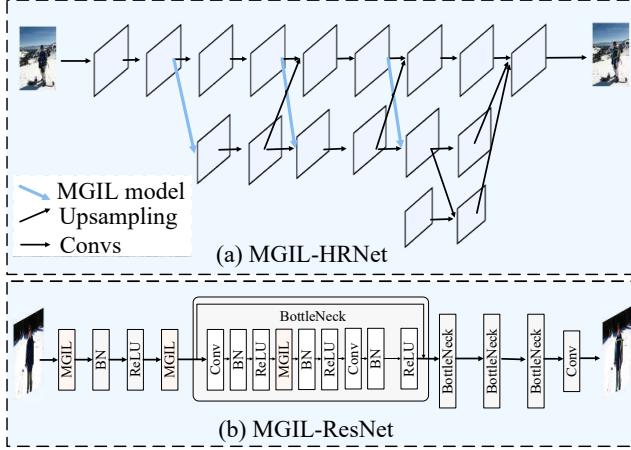


Figure 3: The overall architecture of MGIL-HRNet and MGIL-ResNet.

to virtual scenes. Some works [45, 70] concentrate on end-to-end multi-person pose estimation, making the model more convenient for practical applications. Li *et al.* [74] focuses on researching whole-body keypoints to improve the performance of downstream tasks.

2.2 Low-resolution Vision Tasks

Currently, studies on low-resolution images are emerging [10, 23, 26, 38, 43, 47, 63]. Some studies aim at weakening the impact of quantization error in low-resolution instance detection. For example, the work [60] minimizes the impact of quantization error on the prediction results by means of confidence-aware learning. The work [30] similarly reduces the quantization error in low-resolution images by transforming the coordinate regression method into a classification task. However, these methods only optimize at the label representation level but do not address the lack of valid information in low-resolution images. Other studies [16, 40, 46] are devoted to further optimizing the low-resolution model by distilling the high-resolution feature information to the low-resolution model. Qi *et al.* [40] propose multi-scale aligned distillation for low-resolution detection. By aligning high-resolution features with low-resolution features, it improves the effect of knowledge distillation. Shin *et al.* [46] enhance the performance of low-resolution face detection through attention-based knowledge distillation.

There are some studies aiming to improve the backbone for low-resolution detection. The work [51] proposes SPD-Conv to enhance the performance of low-resolution vision tasks. However, it lacks the utilization of multi-granular information. The traditional method [50] of directly increasing image resolution through upsampling interpolation indeed achieves good performance. However, it leads to a significant increase in Params and GFLOPs, making it impractical for performance-limited devices. In this work, we propose a Multi-Granular Information-Lossless (MGIL) model to solve the above problems. Moreover, we are the first to propose a universal model and apply it to low-resolution human pose estimation.

3 METHODS

We first introduce the overall framework of our MGIL model and then introduce the designed modules in detail.

3.1 Overall Framework

It provides a framework for the proposed model in Fig. 4 (a). The model is composed of a Fine-grained Lossless Information Extraction (FLIE) module, a Coarse-grained Information Interaction (CII) module, and a Multi-Granular Adaptive Fusion (MGAF) mechanism. The FLIE module includes a Space-Channel Transformation (SCT) unit and a Lossless Information Extraction (LIE) block. It is introduced in Sec. 3.2. The CII module consists of a Multi-Receptive Information Extract (MRIE) unit and a Lossless Information Extraction (LIE) block. We describe it in Sec. 3.3. The MGAF mechanism is described in Sec. 3.4.

The model we propose can replace the downsampling layer in the current SOTA models, thereby enabling these models to achieve better performance in low-resolution tasks. Fig. 3 vividly illustrates the overall architecture of applying the MGIL model to HRNet [50] and ResNet [13].

3.2 Fine-grained Lossless Information Extraction (FLIE) Module

For human pose estimation, cutting-edge CNN models commonly use downsampling layers to reduce redundant information and alleviate computational costs. The downsampling layer results in the loss of much fine-grained information in low-resolution images. To address this problem, we design a Fine-grained Lossless Information Extraction (FLIE) module.

The operation of traditional downsampling layers can be expressed as:

$$X' = \text{Down}(X), \quad (1)$$

where $X \in \mathbb{R}^{H \times W \times C}$ denotes the input feature of the downsampling layer, and H , W , and C are the height, width, and the number of channels of the input feature, respectively; $X' \in \mathbb{R}^{H' \times W' \times C'}$ denotes the output feature of the downsampling layer, and H' , W' , C' are the height, width, and the number of channels of the output feature maps, respectively; $H' = H/2$, $W' = W/2$, $C' = C$. The downsampling layer will lead to the loss of feature information. Our model needs to preserve all input feature information. Meanwhile, to directly replace the downsampling layers and easily apply to various CNN models, MGIL needs to maintain consistency with the input and output feature sizes of the downsampling layer. Thereby, we design a space-channel transformation (SCT) unit.

As depicted in Fig. 4 (b), for any input feature $X \in \mathbb{R}^{H \times W \times C}$ of downsampling layer, we start from different pixel points respectively and sample every two pixels:

$$X' = \text{Sample}(X), \quad (2)$$

where $\text{Sample}(\cdot)$ denotes an interval sampling operation, and X' is the output feature of this unit. It can be concretely expressed as:

$$x'_1 = \begin{pmatrix} x_{0,0} & x_{0,2} & \cdots \\ x_{2,0} & \ddots & \vdots \\ \vdots & \cdots & x_{w-2,h-2} \end{pmatrix}, \quad (3)$$

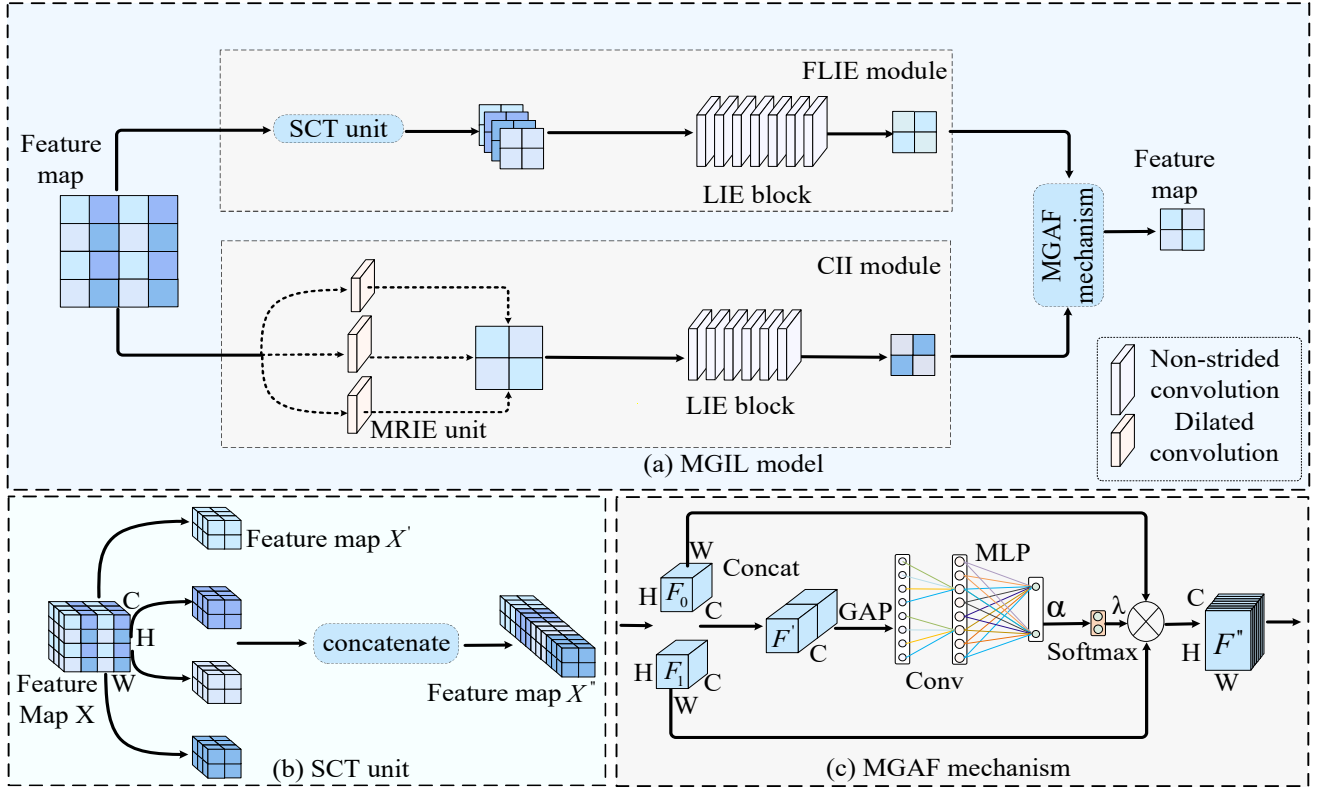


Figure 4: (a) Overview of our proposed MGIL model. The illustration of SCT unit (b) and MGAF mechanism (c).

$$x'_2 = \begin{pmatrix} x_{1,0} & x_{1,2} & \cdots \\ x_{3,0} & \ddots & \vdots \\ \vdots & \cdots & x_{w-1,h-2} \end{pmatrix}, \quad (4)$$

$$x'_3 = \begin{pmatrix} x_{0,1} & x_{0,3} & \cdots \\ x_{2,1} & \ddots & \vdots \\ \vdots & \cdots & x_{w-2,h-1} \end{pmatrix}, \quad (5)$$

$$x'_4 = \begin{pmatrix} x_{1,1} & x_{1,3} & \cdots \\ x_{3,1} & \ddots & \vdots \\ \vdots & \cdots & x_{w-1,h-1} \end{pmatrix}, \quad (6)$$

where x'_i ($i=1,2,3,4$) is the sampling result with different coordinate points as starting points, h and w represent the height and width of the feature map, respectively. Then we concatenate x'_i along the channel dimension after the above process:

$$X'' = \text{Concat}[x'_1, x'_2, x'_3, x'_4], \quad (7)$$

where $\text{Concat}[\cdot]$ is the concatenation operator, and X'' is the result of the concatenation. In this way, while the feature size decreases, the feature information is fully preserved.

After the SCT unit, we further propose a Lossless Information Extraction Module (LIE) block. The LIE block consists of multiple non-strided convolutions. On one hand, non-strided convolutions

can adequately learn feature information through learnable parameters without any feature information loss. On the other hand, they can also reduce the number of channels to maintain consistency with the modified backbone.

By combining the SCT unit and the LIE block, fine-grained feature information is fully utilized. Tab. 5 provides strong evidence of the performance of the FLIE module.

3.3 Coarse-grained Information Interaction (CII) Module

The traditional convolution only focuses on local fine-grained information, as shown in Fig. 2 (b). However, for human pose estimation, the skeletal structure information, the symmetrical relationship information between joints, and the background information all contribute to inferring joint positions. These all require coarse-grained information from the images, rather than the fine-grained information that traditional convolutions focus on. This work designs a Coarse-grained Information Interaction (CII) module to capture coarse-grained information to address the problem.

As shown in Fig. 2 (c), dilated convolution is the operation of enlarging the convolution kernel by adding gaps between its elements. As the convolutional kernel expands, the corresponding receptive field also increases. Dilated convolution helps to capture contextual information on keypoints. We can set different dilation

Table 1: Comparison with SOTA methods on the COCO validation dataset.

Method	Input size	Backbone	AP \uparrow	AP50 \uparrow	AP75 \uparrow	AP(M) \uparrow	AP(L) \uparrow	AR \uparrow
HRNet [50]		HRNet-W32	8.2	36.9	1.3	9.2	6.8	15.0
TokenPose [31]		HRNet-W32	14.0	48.2	3.4	15.2	12.5	21.7
CAL [60]		HRNet-W32	26.4	61.9	18.2	27.1	25.7	33.9
Rle [27]		HRNet-W32	24.4	-	-	-	-	-
Dark [77]		HRNet-W32	12.5	45.2	2.5	13.8	11.1	20.3
SimBase [66]	32x32	ResNet-152	4.4	21.1	1.0	5.3	3.2	9.0
PCT [12]		Swin-Base	1.3	4.6	10.0	1.0	1.2	3.1
Distillpose [75]		HRNet-W32	9.5	32.6	2.4	10.0	9.5	21.2
SimCC(<i>baseline</i>) [30]		ResNet-50	15.7	43.5	8.3	16.5	14.8	21.4
MGIL(<i>ours</i>)		ResNet-50	16.7_{+1.0}	45.1	9.4	17.8	15.5	22.6
SimCC(<i>baseline</i>) [30]		HRNet-W32	29.8	65.6	22.5	30.0	29.9	36.3
MGIL(<i>ours</i>)		HRNet-W32	37.5_{+7.7}	73.9	34.2	37.5	37.9	43.7
SimBase [66]		ResNet-152	30.3	67.6	22.6	30.6	30.5	36.2
Distillpose [75]		HRNet-W32	31.7	66.8	26.6	32.3	31.8	44.5
PCT [12]		Swin-Base	11.8	37.4	4.80	12.2	12.0	17.8
Rle[27]		HRNet-W32	52.5	-	-	-	-	-
HRNet [50]	64x64	HRNet-W48	46.9	83.7	49.2	46.6	47.5	52.6
Tokenpose [31]		HRNet-W48	50.3	82.7	54.4	49.9	51.4	55.6
CAL [60]		HRNet-W48	60.6	88.1	68.4	59.5	62.3	65.5
Dark [77]		HRNet-W48	57.2	86.8	63.5	55.9	59.2	62.2
Simcc(<i>baseline</i>) [30]		HRNet-W48	58.6	85.9	64.9	57.8	60.5	63.4
MGIL(<i>ours</i>)		HRNet-W48	63.1_{+4.5}	88.0	70.7	61.6	65.4	67.5
SimCC(<i>baseline</i>) [30]		HRNet-W32	72.3	91.4	80.1	70.1	76.2	75.7
MGIL(<i>ours</i>)	128x128	HRNet-W32	73.0_{+0.7}	91.4	80.2	70.7	76.7	76.1

rates to obtain various receptive fields, thus capturing multi-scale information about the human body. This will help the model extract more low-resolution human body information.

In this work, we first adopt dilated convolutions to achieve coarse-grained information extraction and interaction. Similar to the FLIE module, to further exploit feature information, we also employ the LIE block within the CII module. Table 7 adequately demonstrates the effectiveness of adding the LIE block to the CII module. The MRIE unit and the CII module complement each other, promoting the utilization of coarse-grained information.

As shown in Fig. 2 (a), the FLIE module ensures the lossless transmission of information and fully learns feature information, and the CII module further learns coarse-grained information. The combination of the two effectively addresses the issue of severe information deficiency in low-resolution images.

3.4 Multi-Granular Adaptive Fusion (MGAF) Mechanism

Usually, the approach to fuse features of different granularities is directly adding them together. However, for features of different granularities, their importance varies. Specifically, for occluded keypoints, the local information at the keypoint is not as important as the contextual information. Because the local information describes occluding objects rather than keypoints. In contrast, contextual information about keypoints becomes more important. In this case, coarse-grained features contain more useful information and should be assigned greater weight.

To solve this problem, inspired by the efficient channel attention (ECA) module [61], we propose a Multi-Granular Adaptive Fusion (MGAF) mechanism. Fig. 4 (c) illustrates the MGAF mechanism. The input for the MGAF mechanism comes from the output feature maps of different granularities. The MGAF mechanism can assign different weights to features at each granularity based on the corresponding output feature information.

As shown in Fig. 4 (c), initially, concatenate the two feature maps along the channel dimension and perform global average pooling to obtain 1D contextual features of:

$$F' = \frac{1}{H \times W} \sum_{i=1}^H \sum_{j=1}^W [F_0, F_1](i, j), \quad (8)$$

where F_0, F_1 are the output feature maps of each granularity respectively, $[\cdot]$ indicates the concatenate operation of feature maps along the channel dimension, and H, W are the height and width of the feature map respectively. The global pooling operations are advantageous for capturing spatial global information of features, which thus aids in the fusion of different features. Then F' is fed into a one-dimensional convolution and then into a fully connected layer to generate the weight matrix:

$$\alpha = MLP(Conv(F')), \quad (9)$$

where $Conv$ is an 1x1 convolution with an adaptive number of output channels. $MLP(\cdot)$ consists of a ReLU function and an FC layer with 2 output channels. The convolution operation can fully learn the correlation between the feature channels. The MLP operator

Table 2: Comparison with SOTA methods on the MPII val dataset.

Method	Input Size	Backbone	Head. \uparrow	Sho. \uparrow	Elb. \uparrow	Wri. \uparrow	Hip. \uparrow	Knee. \uparrow	Ank. \uparrow	PCKh@0.5 \uparrow
SimBase [66]		ResNet-152	89.905	85.258	73.854	64.058	76.216	68.628	62.659	75.353
OKDHP [32]		4-Stack HG	85.573	80.757	66.099	54.328	71.767	61.032	54.393	69.037
HRNet [50]		HRNet-W32	90.075	85.785	72.950	63.511	75.143	67.257	61.880	74.843
Dark [77]		HRNet-W32	89.802	87.568	75.251	64.112	78.726	69.616	63.628	76.612
CAL [60]	64x64	HRNet-W32	92.497	88.689	75.763	65.019	80.076	70.159	65.422	77.692
Tokenpose [31]		HRNet-W32	89.018	86.770	71.570	59.963	77.237	65.947	59.139	73.997
PRTR [28]		HRNet-W32	89.768	83.967	68.144	53.061	76.112	62.039	53.660	70.742
Simcc(<i>baseline</i>) [30]		HRNet-W32	92.701	88.060	76.376	66.198	77.774	68.425	64.076	77.226
MGIL(<i>ours</i>)		HRNet-W32	92.838	89.623	79.461	70.174	80.336	72.033	67.524	79.758^{+2.532}
SimBase [66]		ResNet-152	40.894	48.217	33.953	21.742	44.608	31.353	22.650	36.786
HRNet [50]		HRNet-W32	46.044	52.378	40.191	28.407	48.780	37.176	27.538	42.217
Dark [77]		HRNet-W32	38.984	61.804	46.191	31.867	61.277	45.234	28.839	48.137
CAL [60]		HRNet-W32	77.115	68.631	48.185	33.066	63.164	46.264	40.552	55.353
Tokenpose [31]	32x32	HRNet-W32	38.950	61.702	47.537	31.902	61.676	45.476	28.600	48.421
PRTR [28]		HRNet-W32	0.341	1.512	8.062	9.082	15.977	1.633	0.213	5.618
Simcc(<i>baseline</i>) [30]		HRNet-W32	81.105	72.690	54.219	37.898	63.822	51.380	46.552	59.560
MGIL(<i>ours</i>)		HRNet-W32	87.074	79.721	61.633	47.921	69.275	56.297	51.015	65.948^{+6.388}

Table 3: Performance of our MGIL model in low-resolution object detection tasks on COCO val set.

Method	Backbone	Image size	AP \uparrow
YOLOv5n [18]	YOLOv5	640 \times 640	28.0
YOLOv5-SPD-n [51]	YOLOv5	640 \times 640	31.0
YOLOX-Nano [18]	YOLOv5	640 \times 640	25.3
MGIL(<i>ours</i>)	YOLOv5	640 \times 640	38.7^(+10.7)

Table 4: Performance of our MGIL model in low-resolution image classification tasks.

Model	Dataset	Top-1 accuracy (%) \uparrow
ResNet18 [52]	TinyImageNet	61.68
Nystromformer [67]	TinyImageNet	49.56
WaveMix-128/7 [17]	TinyImageNet	52.03
MGIL(<i>ours</i>)	TinyImageNet	63.61^(+1.93)
ResNet50 [21]	CIFAR-10	93.94
Stochastic Depth [14]	CIFAR-10	94.77
Prodpoly [8]	CIFAR-10	94.9
MGIL(<i>ours</i>)	CIFAR-10	94.20^(+0.26)

serves two purposes: firstly, they reduce the number of feature channels to match the number of granularities. Secondly, they complement convolution operations, further enhancing the learning of

channel correlations, and thereby optimizing weight allocation. Finally, a Softmax operation is applied to the weight matrix to obtain the weight coefficients for different granularities:

$$\lambda = \text{Softmax}(\alpha), \quad (10)$$

where λ is a sequence of 2-dimensional weights. The features of different granularities are combined with their corresponding weight to obtain the final fusion result:

$$F'' = \lambda_0 \cdot F_0 + \lambda_1 \cdot F_1, \quad (11)$$

where λ_0 and λ_1 are the coefficients corresponding to each granularity, respectively, and F'' are the fused features. F'' are then fed into the subsequent network structure. The MGAF mechanism can learn spatial global information and channel correlations from each granularity, adaptively assigning weights to them, and ultimately producing a more effective output.

4 EXPERIMENTS

We first evaluate the proposed MGIL model on two benchmark datasets for human pose estimation: COCO [33] and MPII [1]. Then we present the results of object detection and classification. Ablation studies about the main components of MGIL are also provided to help understand the approach.

4.1 Datasets and Metrics

Human pose estimation datasets. To validate the effectiveness of our proposed MGIL model, we conduct experiments on two popular human pose datasets: COCO [33] and MPII [1]. As one of the largest and most challenging datasets for human pose estimation, the COCO dataset contains more than 200K images and 250K human

Table 5: Ablation studies of each proposed module. Improv. = Improvement. It refers to the improvement of the method relative to the baseline (Simcc [30]). Indivi-improv. = Individual improvement. It refers to the improvement of individual modules compared to the method in the preceding row. The “Simcc+SPD” method refers to our direct application of the SPD module [51] to the Simcc [30]. All experiments use HRNet-W32 as the backbone and take images with 32×32 resolution as input.

Method	FLIE	CII	MGAF	AP ↑	Improv.	Indivi-improv.
Simcc [30]	-	-	-	29.8	-	-
Simcc [30] + SPD [51]	-	-	-	33.6	3.8	3.8
Ours	✓	-	-	36.3	6.5	6.5
Ours	✓	✓	-	36.8	7.0	0.5
Ours	✓	✓	✓	37.5	7.7	0.7

Table 6: Ablation studies of the number of non-strided convolution in the LIE block. “Conv number” refers to the total count of non-strided convolutions within the LIE block of the FILE module.

Method	Conv number	Backbone	Input size	AP ↑
Simcc [30]	-	HRNet-W32	32×32	29.8
Ours	1	HRNet-W32	32×32	33.6
Ours	2	HRNet-W32	32×32	36.3
Ours	3	HRNet-W32	32×32	36.6

instances labeled with 17 keypoints. The COCO dataset is divided into three parts: 57k images for the training set, 5k images for val set, and 20k images for the test-dev set. In this paper, we follow the data expansion in [50]. The MPII dataset contains approximately 25K images including over 40K subjects with annotated body joints, where 29K subjects are used for training and 11K subjects are used for testing. The images are collected using an established taxonomy of everyday human activities from YouTube videos. We adopt the same train/valid/test split as in [78]. In the MPII dataset, each person instance has 16 labeled joints.

Object detection datasets. To evaluate the performance of our model on the object detection task, we adopt the COCO [33] dataset.

Classification datasets. The CIFAR-100 [22] dataset consists of colored natural images with 32×32 pixels. The training and testing sets contain 50K and 10K images, respectively. TinyImageNet [24] is a subset of the ILSVRC-2012 classification dataset and contains 200 classes. Each class has 500 training images, 50 validation images, and 50 test images. Each image is of resolution $64 \times 64 \times 3$ pixels.

Evaluation metrics. For human pose estimation, we follow the standard evaluation metrics for the COCO [33] and MPII [1]. In particular, OKS defines the similarity between different human poses. The OKS-based AP (average precision) is reported for the COCO dataset. The PCK metric refers to the percentage of correct keypoints that lie within a normalized distance of ground truth. We adopt the PCKh@0.5 as our evaluation metric for the MPII dataset, which entails a threshold of 50% of the head diameter.

For object detection, we report the standard metric of average precision (AP) on val2017 under different IoU thresholds [0.5:0.95] and object sizes (small, medium, large). For classification, we use top-1 accuracy as the metric to evaluate classification performance.

4.2 Implementation Details

For all methods used to compare, we replicate them following their original settings in corresponding papers and code. We only modify the image input resolution, while keeping all other settings unchanged. **For all methods, we train and test under the same low resolution.** We adopt the top-down estimation pipeline. We use a commonly used person detector provided by SimpleBaselines [66] with 56.4 AP for the COCO val dataset.

We first train the SOTA models at low resolution and then test them at the same resolution. Experimental results indicate that the Simcc [30] method achieves the best performance. We adopt it as our base model. The training settings for our method, such as the optimizer, learning rate, and data augmentation, are the same as Simcc [30]. All experiments are implemented using the PyTorch library on two NVIDIA GeForce 3080-Ti GPUs.

4.3 Results in Human Pose Estimation

COCO. We replicate the existing SOTA models at different low resolutions. We evaluate our methods on the COCO validation dataset. The experimental results are shown in Tab. 1. We can see that MGIL achieves the best performance compared with other SOTA methods. In particular, we surpass the baseline method (Simcc [30]) by 7.7 mAP. Our method achieves a consistent performance improvement in different resolutions and backbones. It fully demonstrates that our proposed MGIL is an effective and universal model for low-resolution human pose estimation.

MPII. The results on the MPII validation set are shown in Tab. 2. We also conduct experiments at different resolutions. Our approach significantly surpasses the other methods. Compared to the baseline method SimCC [30], our method achieves an improvement of 6.388 under the metric of PCKh@0.5 when the input resolution is 32×32 . It further validates the effectiveness of our approach.

4.4 Results on Other Computer Vision Tasks

Object detection. To demonstrate the generality of our approach, we apply the model to low-resolution object detection tasks and conduct experiments on the COCO dataset, as shown in Tab. 3. We replace the downsampling layer in YOLOv5n with MGIL. Our method outperforms the baseline method by 10.7 mAP. The effectiveness and generality of our MGIL are thoroughly validated.

Classification. In this section, we verify the performance of our MGIL model in low-resolution classification. The experiments are conducted on two datasets: CIFAR-10 and TinyImageNet. Similarly,



Figure 5: Visual results of our model under low-resolution conditions based on the COCO val dataset. From left to right, the resolutions are 128×128 , 128×128 , 128×128 , 64×64 , 64×64 , and 64×64 , respectively.

Table 7: Ablation studies of the LIE block in different modules. “Conv number” refers to the sum of non-strided convolutions.

Method	Conv number in FILE	Conv number in CII	AP
Simcc [30]	-	-	29.8
Ours	1	-	33.6
Ours	1	1	34.6
Ours	2	-	36.3
Ours	2	1	36.8
Ours	2	2	37.1

we replace the downsampling layer with MGIL. As shown in Tab. 4, our method improves the performance of both datasets showing that our method is versatile for low-resolution classification tasks.

4.5 Ablation Studies

Each component. In this subsection, we conduct ablation experiments to demonstrate the contribution of each proposed component. As shown in Tab. 5, all the proposed components contribute to the improvement of the model’s performance. Compared to traditional downsampling layers, the “Simcc+SPD” method improves performance by 3.8 mAP. Our proposed Fine-grained Lossless Information Extraction (FLIE) module, Coarse-grained Information Interaction (CII) module and Multi-Granular Adaptive Fusion (MGAF) mechanism improves performance by 6.5, 0.5, and 0.7 mAP, respectively. The ablation experiments demonstrate the complementary roles of each of our proposed modules, and the combination of all proposed methods results in the best performance, with a significant 7.7 mAP improvement over the baseline.

Conv number in the LIE block. To verify the impact of the number of non-stride convolutions within the LIE block on the module’s performance, we conduct experiments with various numbers of non-stride convolutions. As shown in Tab. 6, as the number of non-strided convolutions increases, the model’s accuracy gradually improves. It indicates that increasing the number of non-strided convolutions allows for further learning of low-resolution information. However, excessive non-strided convolutions also increase the model’s computational cost. Therefore, we choose 3 as the number of convolutions in the LIE block.

LIE block in different modules. The LIE block is composed of several non-strided convolutions. Tab. 7 shows the number of

Table 8: Ablation studies for the Multi-Granular Adaptive Fusion (MGAF) mechanism. “Conv number” refers to the sum of non-strided convolutions.

Method	Conv number in FILE	Conv number in CII	AF	AP \uparrow
Ours	1	1	×	34.6
Ours	1	1	✓	35.7
Ours	2	2	×	37.1
Ours	2	2	✓	37.5

non-strided convolutions in different modules. The results indicate that the LIE block brings substantial improvement in both the FILE and CII modules.

MGAF mechanism. We perform ablation experiments of the Multi-Granular Adaptive Fusion (MGAF) mechanism in different model structures. We realize different model structures by setting the various number of non-stride convolutions in each module. As shown in Tab. 8, relative to the direct additive fusion method, the MGAF mechanism improves 1.1 mAP and 0.4 mAP, respectively. It proves that the MGAF mechanism can further extract effective feature information. It has excellent performance and robustness.

4.6 Visualized Results

Fig. 5 provides more visualized human pose estimation results. As is shown in Fig. 5, the MGIL model achieves accurate human pose estimation when the input is low-resolution.

5 CONCLUSION

In this work, we propose a novel Multi-Granular Information-Lossless (MGIL) model, which can significantly improve the performance of low-resolution vision tasks. Our proposed model adaptively extracts multi-granular feature information, greatly supplementing the effective feature information that originally was not sufficient under low-resolution conditions. Our work truly discovers and addresses the pain points of low-resolution visual tasks. Numerous experiments show its versatility and effectiveness. It can easily replace the downsampling layer in various backbones, various input resolutions, and various low-resolution vision tasks. Next, we plan to extend MGIL to large models to achieve greater improvements in performance on low-resolution vision tasks.

REFERENCES

- [1] Mykhaylo Andriluka, Leonid Pishchulin, Peter Gehler, and Bernt Schiele. 2014. 2d human pose estimation: New benchmark and state of the art analysis. In *Proceedings of the IEEE Conference on computer vision and pattern recognition*. 3686–3693.
- [2] Bruno Artacho and Andreas Savakis. 2020. Unipose: Unified human pose estimation in single images and videos. In *Proceedings of the IEEE/CVF conference on computer vision and pattern recognition*. 7035–7044.
- [3] Vasileios Belagiannis, Christian Rupprecht, Gustavo Carneiro, and Nassir Navab. 2015. Robust optimization for deep regression. In *Proceedings of the IEEE international conference on computer vision*. 2830–2838.
- [4] Adrian Bulat and Georgios Tzimiropoulos. 2016. Human pose estimation via convolutional part heatmap regression. In *Computer Vision—ECCV 2016: 14th European Conference, Amsterdam, The Netherlands, October 11–14, 2016, Proceedings, Part VII 14*. Springer, 717–732.
- [5] Zhe Cao, Tomas Simon, Shih-En Wei, and Yaser Sheikh. 2017. Realtime multi-person 2d pose estimation using part affinity fields. In *Proceedings of the IEEE conference on computer vision and pattern recognition*. 7291–7299.
- [6] Joao Carreira, Pulkit Agrawal, Katerina Fragkiadaki, and Jitendra Malik. 2016. Human pose estimation with iterative error feedback. In *Proceedings of the IEEE conference on computer vision and pattern recognition*. 4733–4742.
- [7] Yilun Chen, Zhicheng Wang, Yuxiang Peng, Zhiqiang Zhang, Gang Yu, and Jian Sun. 2018. Cascaded pyramid network for multi-person pose estimation. In *Proceedings of the IEEE conference on computer vision and pattern recognition*. 7103–7112.
- [8] Grigorios G Chrysos, Stylianos Moschoglou, Giorgos Bouritsas, Jiankang Deng, Yannis Panagakis, and Stefanos Zafeiriou. 2021. Deep polynomial neural networks. *IEEE transactions on pattern analysis and machine intelligence* 44, 8 (2021), 4021–4034.
- [9] Hao-Shu Fang, Shuqin Xie, Yu-Wing Tai, and Cewu Lu. 2017. Rmpe: Regional multi-person pose estimation. In *Proceedings of the IEEE international conference on computer vision*. 2334–2343.
- [10] Shiming Ge, Shengwei Zhao, Chenyu Li, and Jia Li. 2018. Low-resolution face recognition in the wild via selective knowledge distillation. *IEEE Transactions on Image Processing* 28, 4 (2018), 2051–2062.
- [11] Zigang Geng, Ke Sun, Bin Xiao, Zhaoxiang Zhang, and Jingdong Wang. 2021. Bottom-up human pose estimation via disentangled keypoint regression. In *Proceedings of the IEEE/CVF conference on computer vision and pattern recognition*. 14676–14686.
- [12] Zigang Geng, Chunyu Wang, Yixuan Wei, Ze Liu, Houqiang Li, and Han Hu. 2023. Human Pose as Compositional Tokens. In *Proceedings of the IEEE/CVF Conference on Computer Vision and Pattern Recognition*. 660–671.
- [13] Kaiming He, Xiangyu Zhang, Shaoqing Ren, and Jian Sun. 2016. Deep residual learning for image recognition. In *Proceedings of the IEEE conference on computer vision and pattern recognition*. 770–778.
- [14] Gao Huang, Yu Sun, Zhuang Liu, Daniel Sedra, and Kilian Q Weinberger. 2016. Deep networks with stochastic depth. In *Computer Vision—ECCV 2016: 14th European Conference, Amsterdam, The Netherlands, October 11–14, 2016, Proceedings, Part IV 14*. Springer, 646–661.
- [15] Junjie Huang, Zheng Zhu, Feng Guo, and Guan Huang. 2020. The devil is in the details: Delving into unbiased data processing for human pose estimation. In *Proceedings of the IEEE/CVF conference on computer vision and pattern recognition*. 5700–5709.
- [16] Zhenhua Huang, Shunzhi Yang, MengChu Zhou, Zhetao Li, Zheng Gong, and Yunwen Chen. 2022. Feature map distillation of thin nets for low-resolution object recognition. *IEEE Transactions on Image Processing* 31 (2022), 1364–1379.
- [17] Pranav Jeevan and Amit Sethi. 2022. Wavemix: resource-efficient token mixing for images. *arXiv preprint arXiv:2203.03689* (2022).
- [18] Glenn Jocher, Ayush Chaurasia, Alex Stoken, Jirka Borovec, Yonghye Kwon, Kalen Michael, Jiacong Fang, Zeng Yifu, Colin Wong, Diego Montes, et al. 2022. ultralytics/yolov5: v7. 0-yolov5 sota realtime instance segmentation. *Zenodo* (2022).
- [19] Xuan Ju, Ailing Zeng, Jianan Wang, Qiang Xu, and Lei Zhang. 2023. Human-art: A versatile human-centric dataset bridging natural and artificial scenes. In *Proceedings of the IEEE/CVF Conference on Computer Vision and Pattern Recognition*. 618–629.
- [20] Zhehan Kan, Shuoshuo Chen, Ce Zhang, Yushun Tang, and Zhihai He. 2023. Self-Correctable and Adaptable Inference for Generalizable Human Pose Estimation. In *Proceedings of the IEEE/CVF Conference on Computer Vision and Pattern Recognition*. 5537–5546.
- [21] Brett Koonce and Brett Koonce. 2021. ResNet 50. *Convolutional neural networks with swift for tensorflow: image recognition and dataset categorization* (2021), 63–72.
- [22] Alex Krizhevsky, Vinod Nair, and Geoffrey Hinton. 2010. Cifar-10 (canadian institute for advanced research). URL <http://www.cs.toronto.edu/kriz/cifar.html> 5, 4 (2010), 1.
- [23] Jason Kuen, Xiangfei Kong, Zhe Lin, Gang Wang, Jianxiong Yin, Simon See, and Yap-Peng Tan. 2018. Stochastic downsampling for cost-adjustable inference and improved regularization in convolutional networks. In *Proceedings of the IEEE Conference on Computer Vision and Pattern Recognition*. 7929–7938.
- [24] Ya Le and Xuan Yang. 2015. Tiny imagenet visual recognition challenge. *CS 231N* 7, 7 (2015), 3.
- [25] Sohyun Lee, Jaesung Rim, Boseung Jeong, Geonu Kim, Byungju Woo, Haechan Lee, Sunghyun Cho, and Suha Kwak. 2023. Human pose estimation in extremely low-light conditions. In *Proceedings of the IEEE/CVF Conference on Computer Vision and Pattern Recognition*. 704–714.
- [26] Duo Li, Anbang Yao, and Qifeng Chen. 2020. Learning to learn parameterized classification networks for scalable input images. In *Computer Vision—ECCV 2020: 16th European Conference, Glasgow, UK, August 23–28, 2020, Proceedings, Part XXIX 16*. Springer, 19–35.
- [27] Jiefeng Li, Siyuan Bian, Ailing Zeng, Can Wang, Bo Pang, Wentao Liu, and Cewu Lu. 2021. Human pose regression with residual log-likelihood estimation. In *Proceedings of the IEEE/CVF international conference on computer vision*. 11025–11034.
- [28] Ke Li, Shijie Wang, Xiang Zhang, Yifan Xu, Weijian Xu, and Zhuowen Tu. 2021. Pose recognition with cascade transformers. In *Proceedings of the IEEE/CVF conference on computer vision and pattern recognition*. 1944–1953.
- [29] Wenbo Li, Zhicheng Wang, Binyi Yin, Qixiang Peng, Yuming Du, Tianzi Xiao, Gang Yu, Hongtao Lu, Yichen Wei, and Jian Sun. 2019. Rethinking on multi-stage networks for human pose estimation. *arXiv preprint arXiv:1901.00148* (2019).
- [30] Yanjie Li, Sen Yang, Peidong Liu, Shoukui Zhang, Yunxiao Wang, Zhicheng Wang, Wankou Yang, and Shu-Tao Xia. 2022. Simcc: A simple coordinate classification perspective for human pose estimation. In *European Conference on Computer Vision*. Springer, 89–106.
- [31] Yanjie Li, Shoukui Zhang, Zhicheng Wang, Sen Yang, Wankou Yang, Shu-Tao Xia, and Erjin Zhou. 2021. Tokenpose: Learning keypoint tokens for human pose estimation. In *Proceedings of the IEEE/CVF International conference on computer vision*. 11313–11322.
- [32] Zheng Li, Jingwen Ye, Mingli Song, Ying Huang, and Zhigeng Pan. 2021. Online knowledge distillation for efficient pose estimation. In *Proceedings of the IEEE/CVF international conference on computer vision*. 11740–11750.
- [33] Tsung-Yi Lin, Michael Maire, Serge Belongie, James Hays, Pietro Perona, Deva Ramanan, Piotr Dollár, and C Lawrence Zitnick. 2014. Microsoft coco: Common objects in context. In *Computer Vision—ECCV 2014: 13th European Conference, Zurich, Switzerland, September 6–12, 2014, Proceedings, Part V 13*. Springer, 740–755.
- [34] I Scott MacKenzie. 2012. Human-computer interaction: An empirical research perspective. (2012).
- [35] Douglas Morrison, Adam W Tow, Matt Mctaggart, R Smith, Norton Kelly-Boxall, Sean Wade-Mcgee, Jordan Erskine, Riccardo Grinover, Alec Gurman, T Hunn, et al. 2018. Cartman: The low-cost cartesian manipulator that won the amazon robotics challenge. In *2018 IEEE International Conference on Robotics and Automation (ICRA)*. IEEE, 7757–7764.
- [36] Alejandro Newell, Kaiyu Yang, and Jia Deng. 2016. Stacked hourglass networks for human pose estimation. In *Computer Vision—ECCV 2016: 14th European Conference, Amsterdam, The Netherlands, October 11–14, 2016, Proceedings, Part VIII 14*. Springer, 483–499.
- [37] George Papandreou, Tyler Zhu, Nori Kanazawa, Alexander Toshev, Jonathan Tompson, Chris Bregler, and Kevin Murphy. 2017. Towards accurate multi-person pose estimation in the wild. In *Proceedings of the IEEE conference on computer vision and pattern recognition*. 4903–4911.
- [38] Xingchao Peng, Judy Hoffman, X Yu Stella, and Kate Saenko. 2016. Fine-to-coarse knowledge transfer for low-res image classification. In *2016 IEEE International Conference on Image Processing (ICIP)*. IEEE, 3683–3687.
- [39] Duc-Minh Pham. 2018. Human identification using neural network-based classification of periodic behaviors in virtual reality. In *2018 IEEE Conference on Virtual Reality and 3D User Interfaces (VR)*. IEEE, 657–658.
- [40] Lu Qi, Jason Kuen, Jiuxiang Gu, Zhe Lin, Yi Wang, Yukang Chen, Yanwei Li, and Jiaya Jia. 2021. Multi-scale aligned distillation for low-resolution detection. In *Proceedings of the IEEE/CVF Conference on Computer Vision and Pattern Recognition*. 14443–14453.
- [41] Haoxuan Qu, Li Xu, Yujun Cai, Lin Geng Foo, and Jun Liu. 2022. Heatmap distribution matching for human pose estimation. *Advances in Neural Information Processing Systems* 35 (2022), 24327–24339.
- [42] Joseph Redmon, Santosh Divvala, Ross Girshick, and Ali Farhadi. 2016. You only look once: Unified, real-time object detection. In *Proceedings of the IEEE conference on computer vision and pattern recognition*. 779–788.
- [43] Mark Sandler, Andrey Zhmoginov, Andrew Gerald Howard, and Pramod Kaushik Mudrakarta. 2023. Parameter-efficient multi-task and transfer learning. US Patent 11,676,008.
- [44] Saurabh Sharma, Pavan Teja Varigonda, Prashast Bindal, Abhishek Sharma, and Arjun Jain. 2019. Monocular 3d human pose estimation by generation and ordinal ranking. In *Proceedings of the IEEE/CVF international conference on computer vision*. 2325–2334.

- [45] Dahu Shi, Xing Wei, Liangqi Li, Ye Ren, and Wenming Tan. 2022. End-to-end multi-person pose estimation with transformers. In *Proceedings of the IEEE/CVF Conference on Computer Vision and Pattern Recognition*. 11069–11078.
- [46] Sungho Shin, Joosoon Lee, Junseok Lee, Yeonguk Yu, and Kyoobin Lee. 2022. Teaching where to look: Attention similarity knowledge distillation for low resolution face recognition. In *European Conference on Computer Vision*. Springer, 631–647.
- [47] Maneet Singh, Shruti Nagpal, Mayank Vatsa, and Richa Singh. 2021. Enhancing fine-grained classification for low resolution images. In *2021 International Joint Conference on Neural Networks (IJCNN)*. IEEE, 1–8.
- [48] Kai Su, Dongdong Yu, Zhenqi Xu, Xin Geng, and Changhu Wang. 2019. Multi-person pose estimation with enhanced channel-wise and spatial information. In *Proceedings of the IEEE/CVF conference on computer vision and pattern recognition*. 5674–5682.
- [49] Ke Sun, Cuiling Lan, Junliang Xing, Wenjun Zeng, Dong Liu, and Jingdong Wang. 2017. Human pose estimation using global and local normalization. In *Proceedings of the IEEE international conference on computer vision*. 5599–5607.
- [50] Ke Sun, Bin Xiao, Dong Liu, and Jingdong Wang. 2019. Deep high-resolution representation learning for human pose estimation. In *Proceedings of the IEEE/CVF conference on computer vision and pattern recognition*. 5693–5703.
- [51] Raja Sunkara and Tie Luo. 2022. No more strided convolutions or pooling: A new CNN building block for low-resolution images and small objects. In *Joint European Conference on Machine Learning and Knowledge Discovery in Databases*. Springer, 443–459.
- [52] Sasha Targ, Diogo Almeida, and Kevin Lyman. 2016. Resnet in resnet: Generalizing residual architectures. *arXiv preprint arXiv:1603.08029* (2016).
- [53] Zhi Tian, Hao Chen, and Chunhua Shen. 2019. Directpose: Direct end-to-end multi-person pose estimation. *arXiv preprint arXiv:1911.07451* (2019).
- [54] Jonathan J Tompson, Arjun Jain, Yann LeCun, and Christoph Bregler. 2014. Joint training of a convolutional network and a graphical model for human pose estimation. *Advances in neural information processing systems* 27 (2014).
- [55] Alexander Toshev and Christian Szegedy. 2014. Deeppose: Human pose estimation via deep neural networks. In *Proceedings of the IEEE conference on computer vision and pattern recognition*. 1653–1660.
- [56] Ali Varamesh and Tinne Tuytelaars. 2020. Mixture dense regression for object detection and human pose estimation. In *Proceedings of the IEEE/CVF conference on computer vision and pattern recognition*. 13086–13095.
- [57] Ashish Vaswani, Noam Shazeer, Niki Parmar, Jakob Uszkoreit, Llion Jones, Aidan N Gomez, Łukasz Kaiser, and Illia Polosukhin. 2017. Attention is all you need. *Advances in neural information processing systems* 30 (2017).
- [58] Arpita Vats and David C Anastasiu. 2022. Key point-based driver activity recognition. In *Proceedings of the IEEE/CVF Conference on Computer Vision and Pattern Recognition*. 3274–3281.
- [59] Thang Vu, Cao Van Nguyen, Trung X Pham, Tung M Luu, and Chang D Yoo. 2018. Fast and efficient image quality enhancement via desubpixel convolutional neural networks. In *Proceedings of the European Conference on Computer Vision (ECCV) Workshops*. 0–0.
- [60] Chen Wang, Feng Zhang, Xiatian Zhu, and Shuzhi Sam Ge. 2022. Low-resolution human pose estimation. *Pattern Recognition* 126 (2022), 108579.
- [61] Qilong Wang, Banggu Wu, Pengfei Zhu, Peihua Li, Wangmeng Zuo, and Qinghua Hu. 2020. ECA-Net: Efficient channel attention for deep convolutional neural networks. In *Proceedings of the IEEE/CVF conference on computer vision and pattern recognition*. 11534–11542.
- [62] Yihan Wang, Muyang Li, Han Cai, Wei-Ming Chen, and Song Han. 2022. Lite pose: Efficient architecture design for 2d human pose estimation. In *Proceedings of the IEEE/CVF Conference on Computer Vision and Pattern Recognition*. 13126–13136.
- [63] Yikai Wang, Fuchun Sun, Duo Li, and Anbang Yao. 2020. Resolution switchable networks for runtime efficient image recognition. In *Computer Vision–ECCV 2020: 16th European Conference, Glasgow, UK, August 23–28, 2020, Proceedings, Part XV 16*. Springer, 533–549.
- [64] Fangyun Wei, Xiao Sun, Hongyang Li, Jingdong Wang, and Stephen Lin. 2020. Point-set anchors for object detection, instance segmentation and pose estimation. In *Computer Vision–ECCV 2020: 16th European Conference, Glasgow, UK, August 23–28, 2020, Proceedings, Part X 16*. Springer, 527–544.
- [65] Shih-En Wei, Varun Ramakrishna, Takeo Kanade, and Yaser Sheikh. 2016. Convolutional pose machines. In *Proceedings of the IEEE conference on Computer Vision and Pattern Recognition*. 4724–4732.
- [66] Bin Xiao, Haiping Wu, and Yichen Wei. 2018. Simple baselines for human pose estimation and tracking. In *Proceedings of the European conference on computer vision (ECCV)*. 466–481.
- [67] Yunyang Xiong, Zhanpeng Zeng, Rudrasis Chakraborty, Mingxing Tan, Glenn Fung, Yin Li, and Vikas Singh. 2021. Nyströmformer: A nyström-based algorithm for approximating self-attention. In *Proceedings of the AAAI Conference on Artificial Intelligence*, Vol. 35. 14138–14148.
- [68] Tianhan Xu and Wataru Takano. 2021. Graph stacked hourglass networks for 3d human pose estimation. In *Proceedings of the IEEE/CVF conference on computer vision and pattern recognition*. 16105–16114.
- [69] Yufei Xu, Jing Zhang, Qiming Zhang, and Dacheng Tao. 2022. Vitpose: Simple vision transformer baselines for human pose estimation. *Advances in Neural Information Processing Systems* 35 (2022), 38571–38584.
- [70] Jie Yang, Ailing Zeng, Shilong Liu, Feng Li, Ruimao Zhang, and Lei Zhang. 2023. Explicit box detection unifies end-to-end multi-person pose estimation. *arXiv preprint arXiv:2302.01593* (2023).
- [71] Sen Yang, Zhibin Quan, Mu Nie, and Wankou Yang. 2021. Transpose: Keypoint localization via transformer. In *Proceedings of the IEEE/CVF International Conference on Computer Vision*. 11802–11812.
- [72] Wei Yang, Shuang Li, Wanli Ouyang, Hongsheng Li, and Xiaogang Wang. 2017. Learning feature pyramids for human pose estimation. In *proceedings of the IEEE international conference on computer vision*. 1281–1290.
- [73] Jun Yang, Wanli Ouyang, Hongsheng Li, and Xiaogang Wang. 2016. End-to-end learning of deformable mixture of parts and deep convolutional neural networks for human pose estimation. In *Proceedings of the IEEE conference on computer vision and pattern recognition*. 3073–3082.
- [74] Zhendong Yang, Ailing Zeng, Chun Yuan, and Yu Li. 2023. Effective whole-body pose estimation with two-stages distillation. In *Proceedings of the IEEE/CVF International Conference on Computer Vision*. 4210–4220.
- [75] Suhang Ye, Yingyi Zhang, Jie Hu, Liujuan Cao, Shengchuan Zhang, Lei Shen, Jun Wang, Shouhong Ding, and Rongrong Ji. 2023. DistilPose: Tokenized Pose Regression with Heatmap Distillation. In *Proceedings of the IEEE/CVF Conference on Computer Vision and Pattern Recognition*. 2163–2172.
- [76] Ailing Zeng, Xiao Sun, Fuyang Huang, Minhao Liu, Qiang Xu, and Stephen Lin. 2020. Smet: Improving generalization in 3d human pose estimation with a split-and-recombine approach. In *Computer Vision–ECCV 2020: 16th European Conference, Glasgow, UK, August 23–28, 2020, Proceedings, Part XIV 16*. Springer, 507–523.
- [77] Feng Zhang, Xiatian Zhu, Hanbin Dai, Mao Ye, and Ce Zhu. 2020. Distribution-aware coordinate representation for human pose estimation. In *Proceedings of the IEEE/CVF conference on computer vision and pattern recognition*. 7093–7102.
- [78] Feng Zhang, Xiatian Zhu, and Mao Ye. 2019. Fast human pose estimation. In *Proceedings of the IEEE/CVF conference on computer vision and pattern recognition*. 3517–3526.
- [79] Song-Hai Zhang, Ruilong Li, Xin Dong, Paul Rosin, Zixi Cai, Xi Han, Dingcheng Yang, Haozhi Huang, and Shi-Min Hu. 2019. Pose2seg: Detection free human instance segmentation. In *Proceedings of the IEEE/CVF conference on computer vision and pattern recognition*. 889–898.
- [80] Long Zhao, Xi Peng, Yu Tian, Mubbasir Kapadia, and Dimitris N Metaxas. 2019. Semantic graph convolutional networks for 3d human pose regression. In *Proceedings of the IEEE/CVF conference on computer vision and pattern recognition*. 3425–3435.
- [81] Xingyi Zhou, Dequan Wang, and Philipp Krähenbühl. 2019. Objects as points. *arXiv preprint arXiv:1904.07850* (2019).
- [82] Zhiming Zou and Wei Tang. 2021. Modulated graph convolutional network for 3D human pose estimation. In *Proceedings of the IEEE/CVF international conference on computer vision*. 11477–11487.